Rev.Adv.Mater.Sci. 10 (2005) 28-33

CHARACTERIZATION OF NANOSTRUCTURED MATERIALS BY X-RAY LINE PROFILE ANALYSIS

E. Schafler and M. Zehetbauer

Institute of Materials Physics, University of Vienna, Boltzmanngasse 5, A-1090 Vienna, Austria

Received: April 29, 2005

Abstract. For the characterisation of micro- and nanostructures in bulk as well as in loose powder materials the X-ray Line Profile Analysis (XPA) has proven to be an excellent method. In the last two decades not only the evaluation procedures have been improved extensively, but also the instrumentation like X-ray generators, monochromators and detectors have been developed further.
The application of XPA on a variety of nanostructured materials produced by different methods demonstrates the ability to characterise the micro-/nanostructure in terms of structural size and its distribution and lattice defect densities.

1. INTRODUCTION

From strict definition, nanocrystalline materials reveal a microstructure of a characteristic length scale of up to a few tens of nanometers. Materials with an extended range up to a few hundreds of nanometers are called 'ultrafine grained' or 'submicron' materials. These materials still reveal properties of genuine nanocrystalline materials which largely differ from those of single-crystalline and/or conventional polycrystalline matter. In fact, the particular mechanical, magnetic, electronic and other physical properties of nanomaterials are in focus of the actual scientific and technological research. The nature of the major methods for the production of nanocrystalline materials can be classified into two categories: (i) *'bottom-up'* methods (inert gas condensation, electrodeposition, consolidation of powders, crystallization from amorphous materials and (ii) *'top-down'* methods (shock wave loading, Severe Plastic Deformation (SPD)) [1].

'Bottom-up' methods like those of inert gas condensation and electrodeposition provide materials with very small grain sizes down to a few nanometers while the sample dimensions are limited. However, often porosity occurs and impurities are introduced as in case of consolidated powders, strongly deteriorating the good mechanical properties. 'Top-down' methods can yield compact non-porous material, where particularly *Severe Plastic Deformation (SPD)* is of highest technological interest because of its potential to achieve bulk shape nanomaterials. SPD is described as 'intense plastic straining under high imposed pressure' [2]. There exist various methods of SPD which can be classified by their strain paths.

For the characterization of Nanostructured materials one of the main methods is electron microscopy (TEM, SEM), by means of the visualization and quantitative analysis of the size and shape of crystallites and structures.

Corresponding author: E. Schafler, e-mail: schafler@ap.univie.ac.at

X-ray diffraction often is used for qualitative analysis of multiphase and semi-amorphous states. However, increasing the resolution and the counting statistics of the diffraction experiment allows for detailed analysis of the diffraction profiles which provide quantitative information on several intrinsic parameters being characteristic for the material: the coherently scattering domain size as a measure for the smallest unfaulted unit of the material, and the density and arrangement of defects, mostly dislocations. While the former is representing the grain size in the case of nanocrystalline materials produced by e.g. inert gas condensation and electrodeposition, it means the size of a substructure formed within the grains in the case of e.g. ball milled or SPD materials. The parameters describing the lattice defects seems to be most important for the characterization of ball milled or SPD materials but, as one will see, are also useful when investigating materials produced by inert gas condensation and electrodeposition, which still reveal grown-in stacking faults and dislocations from the production process.

This paper aims at some basic principles and the state of the art of the X-ray diffraction line profile analysis (XPA). Furthermore, the capability of this method for the characterisation of nanostructured materials is demonstrated by some selected examples of the actual research.

2. X-RAY LINE PROFILE ANALYSIS (XPA)

The method of X-ray line profile analysis (XPA) has been developed to a powerful tool for the characterisation of microstructures either in the bulk or in loose powder materials. During the last years, the modelling and evaluation procedures as well as the experimental possibilities and techniques have been significantly improved. The new generations of X-ray generators, enhanced focusing and monochromatizing techniques, and last not least the usage of the high brilliant synchrotron radiation allow investigations even in highly distorted and/or plastically deformed materials and with high time and spatial resolution.

The ideal narrow diffraction pattern shows up numerous deviations which are related to the microstructure of the material and are the subject of peak profile analysis: (i) the *peak shift* which is related to internal stresses or planar faults. (ii) the *peak broadening* which indicates crystallite smallness and the presence of microstrains (-stresses), strain (stress) gradients and/or chemical heterogeneities. (iii) the *anisotropic peak broadening* arising from anisotropic crystallite shape or anisotropic strain. (iv) the *peak asymmetries* which are caused by long-range internal (third order) strains (stresses), planar faults or chemical heterogeneities.

The interpretation of peak profiles in terms of microstructural properties becomes more reliable if the results of other methods, e.g. electron microscopy (TEM or SEM) or residual electrical resistivity (RER), are used for comparison. Vice versa the results of other methods can be refined and amended by using those from XPA.

2.1. Strain broadening

According to the kinematical theory of scattering diffraction profiles result from the convolution of the size (S) and distortion (D) profiles. The Fourier transform of this is the Warren-Averbach equation [3]

$$A(L) = A^S(L)\, A^D(L) \qquad (1)$$

in terms of Fourier coefficients $A^i(L)$, L being the Fourier length. This equation has a wide generality and has been theoretically verified by several authors. One of the main challenge related to this equation is the way in which the size Fourier coefficients, $A^S(L)$, and the mean square strain, $\langle \varepsilon_{g,L}^{\,2} \rangle$, as the central part of the Fourier coefficient $A^D(L)$ are interpreted (g is the length of diffraction vector).

It has been shown that the mean square strain does always depend on g as well as L [4,5]. Theoretical models have been developed which are describing the specific contribution of different types of lattice defects (Wilkens, Krivoglaz and others [6,7]). The experimentally observed behaviour of the mean square strain indicated that the major contribution of strain to diffraction peak broadening comes from dislocations.

The g - dependence of the mean square strain is known in diffraction as 'strain anisotropy' [8]. This means that neither the width nor the Fourier coefficients of the diffraction profiles are monotonic functions of the diffraction angle. Two in principle different approaches have been developed so far for the interpretation of strain anisotropy: (i) a phenomenological model based on the anisotropy of the elastic properties of crystals [4], and (ii) the dislocation model based on the mean square strain of dislocated crystals [5]. The dislocation model of $\langle e_{L,g}^{\,2} \rangle$ takes into account that the contribution of a dislocation to strain broadening depends on the relative orientations between the diffraction vector $\boldsymbol{g}$, and the line and Burgers vectors of dislocations, $\boldsymbol{l}$ and $\boldsymbol{b}$, respectively, in a similar way as the contrast of

dislocations in electron microscopy. The anisotropic contrast can be described by contrast factors, C, which can be calculated numerically on the basis of the crystallography of dislocations and the elastic constants of the crystal [6, 9-11]. In the case of a texture free polycrystal, or a loose powder sample, and a random population of all possible Burgers vectors, the individual contrast factors can be averaged over the permutations of the *hkl* indices. It can be shown that the average contrast factor, $\overline{C}$, is a linear function of the fourth order invariants of the *hkl* indices [12]. In the case of cubic and hexagonal crystals this can be written as:

$$\overline{C} = \overline{C}_{h00}(1 - qH^2)$$

and (2)

$$\overline{C}_{hk.l} = \overline{C}_{hk.0}\,[1 + q_1 x + q^2 x^2],$$

respectively, where $\overline{C}_{h00}$ and $\overline{C}_{hk.0}$ are the average dislocation contrast factors for the *h*00 and *hk*0 reflections, respectively, $H^2 = (h^2k^2 + h^2l^2 + k^2l^2) / (h^2 + k^2 + l^2)^2$; q, q_1 and q_2 are parameters depending on the elastic constants and on the character of dislocations in the crystal (e.g. edge or screw, or basal, prismatic or pyramidal, respectively). In the case of hexagonal crystals, $x = (2/3)(l/ga)^2$ in Eq. (2) where l and a are the prismatic index and the basal lattice constant, respectively. Detailed accounts and compilations of the q, q_1 and q_2 parameters can be found in [10,11]. A phenomenological interpretation of anisotropic strain broadening is given by Stokes and Wilson [13] and Stephens [14].

Recently the theoretical framework for strain evaluation by means of XPA has been further improved by Ungar *et al.* [5] by taking into consideration the influences of stacking faults to the Bragg profile which have been described in detail by Warren [15]. In principle this opens the possibility to determine the density of stacking faults in addition to that of dislocations.

2.2. Size broadening

Size broadened profiles can be described by assuming (i) a size distribution function and (ii) the shape of crystallites, or coherently scattering domains. A log-normal distribution is given by the median m and the variance σ_0. Hinds [16] has shown that the average crystallite diameters are given by

$$\langle x \rangle_k = m \exp(k\sigma^2)\,, \qquad (3)$$

where k = 0.5, 2.5 and 3.5 in the case of arithmetic-, area- and volume weighted averages. Krill and Birringer [17] have proofed this the crystallite size distribution by an investigation of nanocrystalline Pd produced by inert gas condensation and subsequent consolidation.

2.3. Planar faults

Warren has shown that if stacking faults and/or twin-boundaries are present in the crystal, the apparent particle size becomes smaller than the true particle size [15]. Numerical values can be found in Table 1 in the same paper [15] taking into account the order dependence of the effect. These numerical values have been denoted with $W(g)$ [5,18], the density of stacking faults α and twin boundaries β are combined in a variable β'. Then the contribution to broadening from faulting and twinning is determined by $\beta' W(g)$.

2.4. Peak asymmetry

The peak asymmetries indicate the presence of long-range internal stresses of 3rd order, in correspondence with the composite model of Mughrabi [19] describing the heterogeneous dislocation distribution in terms of dislocation poor (cell interiors) and dislocation rich (cell walls) regions. The hard cell wall- and the soft cell-interior materials are put under the forward and backward long-range internal stresses alternating concomitantly with the spatial variation of high and low dislocation densities. The spatial variation of the long-range internal stresses e.g. impose a spatially varying tetragonal distortion on the cubic lattice of copper. The peak asymmetry is the manifestation of this varying tetragonality. The evaluation method of the long-range internal stresses which is based on the composite model makes use of the whole profile description of dislocated crystals [20].

2.5. Evaluation procedure

Evaluation procedures have been developed which provide, beside the 3rd order stresses, the following physical parameters in the case of cubic, or hexagonal crystals, respectively [21,22]: the mean m and the variance σ of the log-normal size distribution function, the dislocation density ρ and the dislocation arrangement parameter $M = R_e\sqrt{\rho}$ (with R_e as the outer cut-off radius of the dislocation strain field), one (cubic) or two parameters (hexagonal) being part of the dislocation contrast factor (Eq. (2)) and the planar fault probability β'.

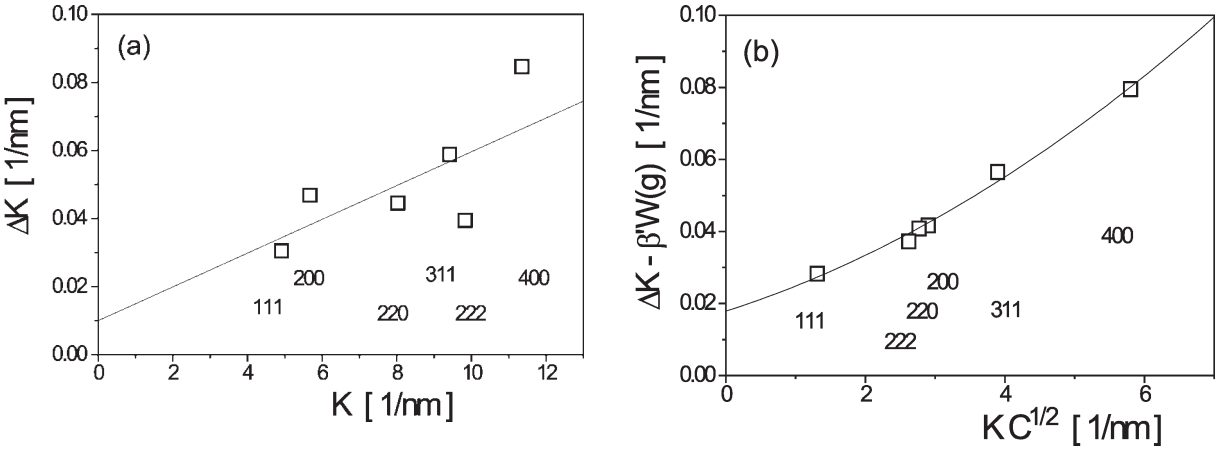

Fig. 1.(a) The conventional Williamson-Hall plot of nanocrystalline electro-deposited Ni. The FWHM of the individual reflections show no monotonic behaviour with the wave number *K*. (b) The modified Williamson-Hall plot of the same data like in (a). The contrast correction scales the abscissa resulting in a monotonic increase of the FWHM.

3. RESULTS AND DISCUSSION

3.1. Electrodeposited Ni

Electrodeposited (ED) nanocrystalline Ni foils were produced by pulse plating onto titanium substrate [23]. Six reflections were measured and the classical Williamson Hall method was applied [24]. In Fig. 1a the non-monotonic increase of the broadening with increasing absolute value of the diffraction vector can be seen, indicating present microstrains. This non-monotonic behaviour is ascribed to the particular contrast conditions. Extrapolating without contrast correction to K=0 yields a value for the average crystallite size of 90 nm. By applying the modified Williamson-Hall approach [25] the strain anisotropy is considered in terms of dislocation contrast and the resulting deviation from monotonic behaviour of ΔK vs. $K{\cdot}C^{1/2}$ is markedly lower. In order to receive a perfectly monotonic curve the influences of planar faults on the broadening must be considered for the evaluation of measured profiles, too (Fig. 1b), which have been grown in during the deposition process. Now a particle size of 50 nm resulted from the XPA which is markedly different from the size evaluation without contrast correction but in good correspondence with findings from TEM [23]. Under the assumption that during the deposition process no deformation but only twin stacking faults are produced, the frequency of twin boundaries is obtained to be 0.0012. The average density of dislocations results to be $4.9{\cdot}10^{15}$ m^{-2}, and most probably these are also grown-in defects formed during the deposition procedure.

3.2. Inert gas condensed Cu

Nanocrystalline Cu was prepared by inert gas condensation and subsequent compaction with 1.4 GPa pressure at 69 °C at Argonne National Laboratory [5]. Six reflection were measured and subjected to the Williamson-Hall procedure. Again a strong strain anisotropy was determined. The appropriate contrast correction as well as the consideration of planar faults were necessary to obtain serious results. The root-mean-squared strains could be explained by the presence of dislocations with a density of $5{\cdot}10^{15}$ m^{-2} of mainly screw character, which may be caused by the particle growth mechanism. The size distribution was rather narrow with means between 14 nm and 30 nm in good correlation with results from transmission electron microscopy. It has been concluded that no deformation stacking faults are present, thus a twin probability of 0.016 is obtained.

3.3. Ni_5Hf crystallized from the amorphous state

Nanocrystalline Ni_5Hf particles were produced by careful crystallization from the amorphous state. The amorphous ribbons of 3 mm width and 11 mm thickness were produced from a master alloy of $Hf_{11}Ni_{89}$ melted and rapidly quenched by the melt-spinning technique. The diffraction patterns show a strong

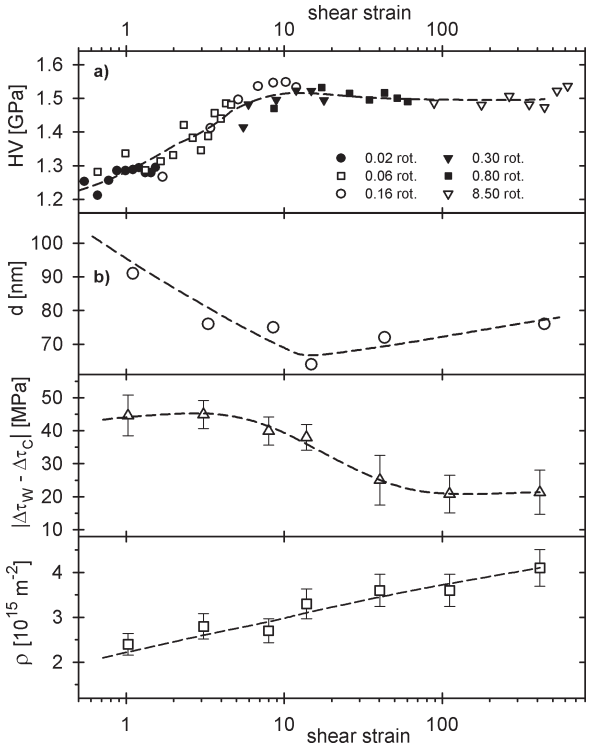

Fig. 2. Several investigated parameters as a function of the resolved shear strain *g* of high pressure torsion deformed Cu: (a) microhardness. (b) coherently scattering domain size; (c) long range internal stresses; (d) dislocation density.

amorphous halo and well defined Debye-Scherrer rings indicating the coexistence of the amorphous and crystalline phases [26]. The crystallite size distribution function determined by XPA revealed values of the median and variance of: m=3.3±0.2 nm and s=0.82±0.02. The arithmetic-and the area-weighted mean crystallite size calculated from m and s according to Eq. (3) are 5 nm and 17 nm respectively. This indicate a wide size distribution in good correlation with the TEM observations where very small and somewhat larger particles appeared.

3.4. Ball milled Ni

High purity Ni powder was ball milled for 96 hours in a planetary mill [22]. Dark field and HREM micrographs were evaluated quantitatively. The dislocation density determined by XPA using the dislocation based model was increasing with milling time and seemed to reach a saturation level after 96 h at about $2.4 \cdot 10^{16}$ m^{-2}. The arithmetic average size is about 10 nm and the distributions obtained by XPA were found to be in very good correlation good correlation with the TEM investigations.

3.5. Severely plastically deformed Cu

Fig.2a shows the dependence of microhardness of Cu deformed by high pressure torsion (HPT) under a pressure of 8 GPa. The microhardness data were taken from different sites of 6 Cu specimens which were deformed by different numbers of rotations. It can be seen that at relatively low resolved shear strains $\gamma \leq 10$, the HPT deformation results in a significant rise of microhardness to a level which is about 30% higher than that can be reached by conventional cold-work [27]. When correlating the microhardness results to the sizes of the coherently scattering domains determined by XPA a Hall-Petch relation follows having two sections with different slopes [28]. Here for the first time it has been shown that in case of severely plastically deformed materials the coherently scattering domains turned out to be the structural element determining the macroscopic strength. Further parameters like the long range internal stresses and the dislocation density are indicating a change of the dislocation wall structure. While more and more dislocation are produced and stored the internal stress level starts to decrease around a shear strain of 10. This only can be explained with a general rearrangement of the dislocation walls which transform into a subgrain like tilt wall structure.

3.6. Deformed polypropylene

The XPA is not restricted to deformed metals with high symmetry lattice type, but also can be applied to polymer materials. The authors have employed it in order show the evidence of dislocations in this semi-crystalline material [29]. Isotactic a-polypropylene has been deformed by rolling deformation up to true strains of ε=0.5 (where $\varepsilon=\ln(d_0/d)$, d_0 and d are the initial and the final sample thickness after rolling, respectively). Five reflections could be measured and the standard Williamson Hall plot like in Fig. 1a exhibited the strong strain anisotropies. Polypropylene has a monoclinic unit cell with one elongated axis and one axis angle slightly differing from 90°. For simplification, a orthorhombic crystal structure has been assumed to reduce the number of independent parameters in the contrast calculation, and still 5 parameters determining the contrast conditions had to be taken into account. For this purpose a combination of the Williamson-Hall approach [24] and the dislocation based Wilkens

model [6,21] has been applied. Considering all physical restrictions, solutions could be found satisfying the demand of the modified Williamson Hall plot. The comparatively high value of the dislocation density of up to $2 \cdot 10^{16}$ m^{-2} can be explained easily when considering the short mean free path of the dislocations of about 20 nm, which is identical to the lamella thickness. This strongly hints on dislocation glide as basic mechanism of the plastic deformation.

4. SUMMARY

The X-ray line profile analysis (MXPA) has been proven to be an excellent method to obtain numerous structural parameters of nanomaterials which are essential for the characterisation and understanding of the enhanced properties. The method carefully can differentiate between size broadening and lattice defect broadening, and provides a reliable determination of grain size and its distribution. It furthermore allows for the absolute measurement of density of dislocations and/or stacking faults, their arrangement and the long range stresses related.

REFERENCES

[1] C.C. Koch, *Nanostructured Materials – Processing, Properties and Potential Application* (Noyes–William Andrew Publ., Norwich, N.Y., USA, 2002).
[2] R.Z. Valiev, In *Investigations and Applications of SPD*, ed. by T.C. Lowe and R.Z. Valiev (Kluwer Academic Publishers, 2000) p.221.
[3] B.E. Warren and B.L. Averbach // *J. Appl. Phys.* **23** (1952) 497.
[4] T. Ungar and A. Borbely // *Appl. Phys. Letters* **69** (1996) 3173.
[5] T. Ungar, S. Ott, P.G. Sanders, A. Borbely and J.R. Weertman // *Acta Mater.* **10** (1998) 3693.
[6] M. Wilkens, In: *Fundamental Aspects of Dislocation Theory*, ed. by J.A. Simmons, R. de Wit and R. Bullough (Vol. II. Nat. Bur. Stand. Spec. Publ. No. 317, Washington DC. USA 1970) p. 1195.
[7] M.A. Krivoglaz, *X-ray and Neutron Diffraction in Nonideal Crystals* (Springer-Verlag, Berlin Heidelberg New York, 1996).
[8] G. Cagliati, A. Paletti and F.P. Ricci // *Nucl. Instrum.* **3** (1958) 223.
[9] P. Klimanek and R. Kuzel Jr. // *J. Appl. Cryst.* **21** (1988) 59.
[10] T. Ungar, I. Dragomir, A. Revesz and A. Borbely // *J. Appl. Cryst.* **32** (1999) 992.
[11] I. Dragomir and T. Ungar // *J. Appl. Cryst.* **35** (2002) 556.
[12] R.E. Dinnebier, R. Von Dreele, P.W. Stephens, S. Jelonek and J. Sieler // *J. Appl. Cryst.* **32** (1999) 761.
[13] A.R. Stokes and A.J.C. Wilson // *Proc. Phy. Soc. London* **56** (1944) 174.
[14] P.W. Stephens // *J. Appl. Cryst*. **32** (1999) 281.
[15] B.E. Warren // *Progr. Metal Phys.* **8** (1959) 147.
[16] W.C. Hinds, *Aerosol Technology: Properties, Behavior and Measurement of Airbone Particles* (Wiley, New York 1982).
[17] C.E. Krill and R. Birringer // *Phil. Mag. A* **77** (1998) 621.
[18] T. Ungar, A. Revesz and A. Borbely // *J. Appl. Cryst.* **31** (1998) 554.
[19] H. Mughrabi // *Acta metall.* **31** (1983)1367.
[20] T. Ungar, I. Groma and M. Wilkens // *J. Appl. Cryst.* **22** (1989) 26.
[21] G. Ribarik, T. Ungar and J. Gubicza // *J. Appl. Cryst.* **34** (2001) 669.
[22] P. Scardi and M. Leoni // *Acta. Cryst. A* **58** (2002) 190.
[23] E. Toth-Kadar, I. Bakonyi, L. Pogany and A. Cziraki // *Surf Coat. Technol.* **88** (1996) 57.
[24] G.K. Williamson and W.H. Hall // *Acta Metall.* **1** (1953) 22.
[25] T. Ungar and A. Borbely // *Appl. Phys. Letters* **69** (1996) 3173.
[26] J. Gubicza, G. Ribarik, I. Bakonyi and T. Ungar // *J. Nanosci. and Nanotechn.* **1** (2001) 343.
[27] M.Zehetbauer and D.Trattner // *Mater.Sci.Eng. A* **89** (1987) 93.
[28] I. Dubravina, M. Zehetbauer, E. Schafler and I. Alexandrov // *Mater.Sci.Eng. A* **387-389** (2004) 817.
[29] H. Wilhelm, A. Paris, E. Schafler, S. Bernstorff, J. Bonarski, T. Ungar and M. J. Zehetbauer// *Mater. Sci. Eng. A* **387-389** (2004) 1018.